Magnetic phase diagram of Ho/Er alloys

R. A. Cowley, J. A. Simpson, C. Bryn-Jacobsen, R. C. C. Ward, and M. R. Wells
Oxford Physics, Clarendon Laboratory, Parks Rd, Oxford OX1 3PU, United Kingdom

D. F. McMorrow
Condensed Matter Physics and Chemistry Department, Risø National Laboratory, DK-4000 Roskilde, Denmark
(Received 25 February 1997; revised manuscript received 29 October 1997)

The magnetic structures of a series of Ho/Er alloys have been determined by neutron-diffraction techniques. The alloys were prepared as thin films (10 000 Å thick) by molecular beam epitaxy, and are single crystals with a mosaic spread of about 0.2°. A variety of magnetic structures are found, arising from the competition between the exchange and anisotropic crystal-field interactions, the latter of which are of opposite sign for Ho and Er. The magnetic phase diagram has five distinct phases with long-range magnetic order: basal-plane helical, tilted helical, cycloidal, *c*-axis longitudinally modulated, and conical. The cycloid and tilted helix have both incommensurate and commensurate $q=\frac{1}{4}c^*$ forms, and all of the thin films have a conical structure at low temperatures, even though corresponding films of pure Ho and Er do not exhibit this phase. There is a *pentacritical point*, and probably a disordered phase which is completely surrounded in the phase diagram by magnetic phases with long-range order. A Landau theory is developed to describe these results. [S0163-1829(98)05414-9]

I. INTRODUCTION

The magnetic structures of the rare-earth metals are complex because of the competition between the exchange interaction, which usually favors structures that are incommensurate with the underlying hexagonal lattice, and the crystal-field interaction, which favors alignment of the magnetic moments along specific crystallographic axes. In this paper we report on the structures of alloys of Ho with Er. Ho and Er have similar exchange interactions but very different crystal-field interactions, and so the study of these alloys enables us to probe the behavior when, on average, the crystal-field interactions become very small and a variety of different magnetic structures are stable.

Both Ho and Er have magnetic structures in which the magnetic moments within each basal plane are aligned ferromagnetically, but the direction and possibly the magnitude of the ordered moments changes from one plane to the next along the *c* axis. The magnetic structures of bulk Er were first determined by Cable *et al.*[1] Between the temperatures of 85 and 52 K, the structure is a *c*-axis longitudinally modulated structure with a wave vector *q* of about $\frac{2}{7}c^*$, and both the moment direction and wave vector are parallel to the *c* axis. Between 52 and 20 K, both the *c* axis and basal-plane components of the moments order to form a cycloidal structure,[2] while the wave vector decreases on cooling from $\frac{2}{7}c^*$ to $\frac{1}{4}c^*$. At 20 K there is a first-order transition to a conical structure in which the ferromagnetic moment is along the *c* axis, the cone angle is about 26°, and the modulation wave vector of the basal-plane components is $\frac{5}{21}c^*$. The magnetic structures of bulk Ho were determined by Koehler *et al.*[3] Between 132 and 20 K, the structure is a basal-plane helix described by a wave vector varying between $\frac{2}{7}c^*$ and $\frac{1}{6}c^*$. At 20 K there is a transition to a conical structure in which the cone angle is about 83°, the rotation of the basal-plane components is described by a wave vector of $\frac{1}{6}c^*$, and there is a bunching of the moments towards the *a* axes in the basal plane.

Since the initial measurements there have been many more detailed studies of the structures of Ho and Er. High resolution x-ray-scattering measurements have revealed long-period commensurate structures in both the cycloidal phase of Er (Ref. 4) and helical phase of Ho (Ref. 5) and detailed studies of these commensurate structures have been made.[2,6,7] These show a variety of distortions of the simple phases described above caused both by the competition between the crystal-field and the exchange interactions, and also by the effect of trigonal interactions which distinguish between the two different sites of the hexagonal crystal structure.

The development of molecular beam epitaxy (MBE) techniques has made possible the growth of high-quality thin films for many materials that are not readily available as bulk single crystals. Although bulk single crystals have been grown by strain annealing, we chose to use single crystal thin films of Ho/Er alloys grown using MBE techniques, as described in the next section. Samples of thin films of Er and Ho have been studied[8,9] and their properties are similar to those of the bulk materials, except that in both cases the conical phase is suppressed. In the case of Ho thin films, the helical phase persists to at least 4 K with a wave vector which increases with decreasing film thickness, and for a thickness of 10 000 Å the wave vector is about $\frac{1}{5}c^*$ at low temperatures. The magnetic structure of a 10 000 Å film of Er at low temperatures is a cycloid with a wave vector of $\frac{1}{4}c^*$. The suppression of the conical phase in the films results, presumably, from the clamping of the rare-earth film by the substrate and the cap, which reduces the gain in the magnetoelastic energy on entering the conical phase. We also note that superlattices of Ho/Er have been studied, and display an unusual coexistence of short and long-range magnetic correlations.[10,11]

Bulk alloys of Ho and Er have been studied by Bozorth *et al.*[12] using magnetization measurements. Their results showed that the onset of magnetic order varies continuously with the concentration between Ho and Er, and that the transition to a conical structure at low temperatures occurs at a higher temperature in the alloys than in the pure materials. A bulk alloy containing equal amounts of both Ho and Er has been studied by neutron[13–15] and x-ray-scattering techniques[16] to determine the magnetic structures, while neutron-scattering measurements have been made of the magnetic structures for a crystal containing 90% of Ho.[13,15] The results show a variety of magnetic structures but did not establish the nature of the phase diagram. We shall discuss these results and compare them with ours for thin films in Sec. IV.

The next section of the paper describes the growth of the alloy samples, the neutron-scattering techniques used to study the magnetic scattering from the alloys, and the analysis of this scattering to determine the magnetic structures. The experimental results are described in detail in Sec. III, where the different magnetic structures are deduced as a function of temperature. There are at least nine different magnetic phases, and it is suggested that one of these phases is disordered and entirely surrounded in the phase diagram by phases with long-range order. A Landau theory is developed in Sec. IV to describe the structures which occur at the onset of magnetic ordering, and the phase diagram is obtained with several multicritical points at one of which five different magnetic phases are stable. At low temperatures, the structures are determined by the energy of the system, and an expression for the energy is obtained and shown to be capable of describing the observed structures. Finally, a summary is given in Sec. V, and the questions raised by this work are further discussed.

II. SAMPLE GROWTH AND NEUTRON SCATTERING

A. Sample growth

The alloys of Ho/Er were grown at Oxford using the MBE techniques described previously.[17] Sapphire substrates with an area of 12×10 mm^2 were UHV annealed and 1300 Å of Nb deposited on them to provide a chemical buffer between the sapphire and the reactive rare earths. 1800 Å of nonmagnetic Y was deposited on the Nb to provide a seed with a growth plane having a similar structure and lattice parameter to the basal plane of the rare earths. Ho and Er were simultaneously deposited onto the seeds with the elemental deposition rates chosen to produce the desired alloy composition, and to grow each alloy at a rate of 1 Å s^{-1} to a thickness of 10 000 Å. During the growth of the alloy, the temperature of the substrate was held at 870 K: a temperature chosen to be high enough to facilitate the growth of high-quality films but sufficiently low to prevent separation of the two rare earths. Finally, 150 Å of Y was deposited to inhibit oxidation of the alloy. Five different samples of the Ho_xEr_{1-x} alloys with nominal compositions $x=0.8$, 0.65, 0.5, 0.3, and 0.1 were grown and their properties investigated.

The samples were studied by x-ray-scattering techniques which showed that the Ho/Er alloys were of single crystal form with the c axis perpendicular to the plane of the films. The Y seed and the alloy had different a-lattice parameters and these were each within error the same as those of the bulk materials. The Y and the alloys were, however, aligned with their crystallographic axes in the same directions. The mosaic spreads of the alloys varied between 0.1° and 0.2° which are typical of the best rare-earth thin films grown in this way.[9,10,17]

TABLE I. Lattice parameters a and c in Å of Ho/Er thin films at 10 K as a function of concentration x.

Conc. x	1[16]	0.93	0.65	0.57	0.31	0.13	0 [17]
a	3.580	3.5707	3.5790	3.5659	3.5609	3.5678	3.555
c	5.621	5.6270	5.618	5.6070	5.5958	5.5950	5.577

One problem has been to find an accurate way of confirming the compositions of the alloys. This is difficult because Ho and Er differ by only one in atomic number and so the x-ray-scattering form factors are very similar. In addition, the neutron-scattering lengths differ by only 0.6%. The lattice parameters of the films, as determined at 15 K, are listed in Table I and compared with those of 10 000 Å films of Ho (Ref. 9) and of Er (Ref. 8). The difference in both the a- and c lattice parameters for Ho and Er is only 0.5% and so these neutron-scattering measurements do not provide an accurate determination of the concentration by using Vegard's Law. We shall return to a discussion of the concentrations in Sec. IV B, but meanwhile we shall refer to the concentrations of the different samples by the best estimate of the concentrations obtained in Sec. IV B and listed together with the nominal concentrations in Table II. Thin films grown by the same method[17] were uniform in concentration to $\pm0.5\%$, and our results are consistent with the Ho/Er alloys having a similar uniformity.

B. Neutron scattering

The neutron-scattering experiments were performed using triple-axis spectrometers at the DR3 reactor of the Risø National Laboratory. Neutrons from a cold source were Bragg reflected from the (002) planes of a pyrolytic graphite monochromator to produce a neutron beam with a wavelength of 4.05 Å. The neutrons with wavelengths of $\lambda/2$, $\lambda/3$, etc. were suppressed by a cooled Be filter. An analyser also of pyrolytic graphite was set to detect elastically scattered neutrons and was used to improve the instrumental resolution and to reduce the background. For three of the samples, $x=0.31$, 0.57, and 0.93, the spectrometer TAS 6 was used with collimation from the reactor to detector of 30′, 29′, 52′, and 104′ giving a resolution in the scattering plane of typically 0.011 Å both parallel and perpendicular to the wave-vector transfer. The remaining two samples and the $x=0.93$ sample were studied using the TAS 1 spectrometer with collimations of 140′, 30′, 60′, and 140′, giving a resolution of 0.021 Å^{-1} parallel and 0.016 Å^{-1} perpendicular to the wave-vector transfer.

The samples were mounted in a variable temperature cryostat with the a^*- and c^*-crystallographic axes in the horizontal-scattering plane. The temperature was controlled to ±0.5 K between 8 and 150 K. Most of the measurements were performed by scanning the wave-vector transfer along the $[0\ 0\ \ell]$ and $[1\ 0\ \ell]$ directions in reciprocal space, while

TABLE II. Transition temperatures in K and magnetic structures of Ho_xEr_{1-x} alloys. Note: The data for $x=0$ and 1 are from Refs. 8,9,17. The phase transition temperatures T_{AB} are for transitions between phase A high temperature and B low temperature where P=paramagnetic, $L=c$-axis longitudinally modulated, C=cycloidal, H=basal-plane helix, T=tilted helical, D=isotropic disordered, and Co=lowest temperatures conical phase. The wave vectors are in units of c^*, and q_C and θ are for the conical phase at low temperatures.

x	0	0.13 (2)	0.31 (2)	0.57 (3)	0.65 (2)	0.93 (2)	1.0
Nominal x	0	0.1	0.3	0.5	0.65	0.8	1.0
T_{PL}	85.6 (4)	88.0 (5)					
T_{PH}			95.0 (5)	109.6 (5)	113.5 (5)	128.9 (4)	133.3 (5)
q_0	0.283	0.284	0.282	0.282	0.281	0.279	0.278
T_{LC}	50 (5)	73.6 (9)					
T_{HT}			81 (1)	45 (2)			
T_{TC}			65 (5)				
Lock-In	20 (4)	27 (1)	35 (1)	45 (2)			
T_{TD}				38 (2)			
T_{CCo}		16.5 (10)	22 (2)				
$T_{DCo}T_{HCo}$				30 (1)	35 (1)	20 (1)	
θ		39.5 (3)	45 (1)	57 (1)	62 (2)	75 (2)	
q_C	0.25	0.241	0.238	0.230	0.224	0.200	0.200

keeping the energy transfer fixed at zero. Particular emphasis was put on the structural Bragg reflections (0 0 2) and (1 0 0) and the magnetic scattering at the (0 0 $2-q$) and (1 0 q) positions in reciprocal space, where q is the modulation wave vector of the magnetic ordering which is always parallel to the [0 0 ℓ] direction and will be given in units of the reciprocal lattice vector c^*.

C. Data analysis

A typical result for the neutron scattering measured in these experiments is shown in Fig. 1 for the $x=0.65$ alloy at a temperature of 9 K. The scattering is dominated by sharp peaks that are mostly resolution limited and from the intensities of these peaks the magnetic structure can be determined. There are a few less intense peaks also illustrated in Fig. 1 which arise from higher order distortions of the ideally harmonic structure. These were only observed at the lowest temperatures.

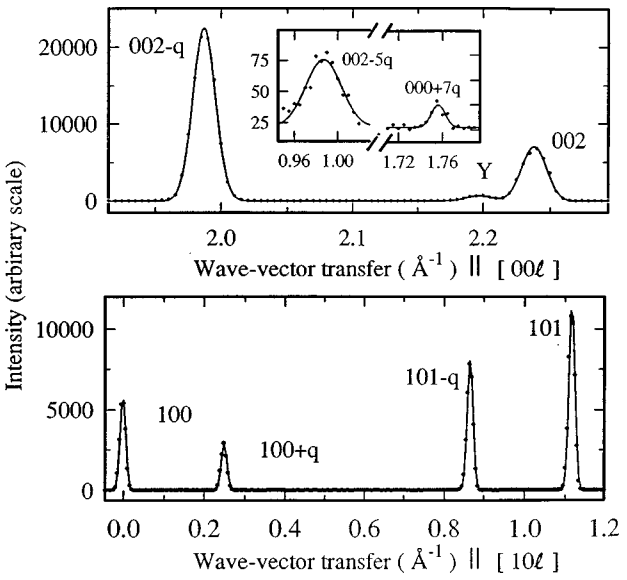

FIG. 1. The scattering observed from $Ho_{0.65}Er_{0.35}$ at 20K. The inset in the upper diagram shows the scattering from the higher harmonics and the label Y shows the scattering from the (0 0 2) reflection of the Y seed.

The principal peaks corresponding to the structural Bragg reflections (0 0 2) and (1 0 0) and to the magnetic scattering occurring at wave vectors (0 0 $2-q$) and (1 0 q) were fitted to Gaussians to obtain their position, width, and integrated intensity. The difference in the position of the nuclear and magnetic scattering gives the modulation wave vector q and these are shown in Fig. 2 for all of the samples. The modulation wave vector q was determined from the (0 0 $2-q$) and (1 0 q) peaks to an accuracy of ± 0.002. The results were within error the same for both peaks except for the $x=0.13$ sample as described in Sec. III F.

Magnetic Bragg scattering provides a measure of the square of the ordered magnetic moment perpendicular to the

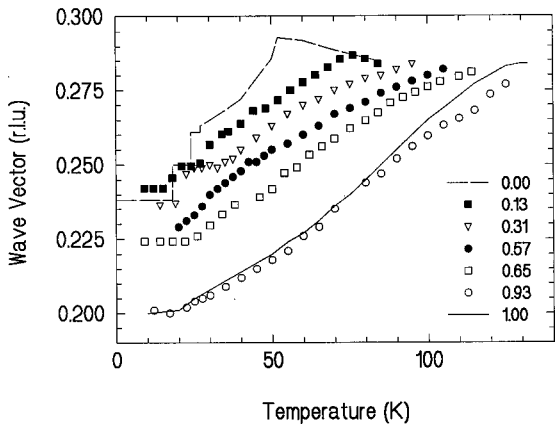

FIG. 2. The wave vectors of the modulated ordering for Ho/Er alloys. The solid line shows the wave vectors for a Ho film (Ref. 17) and the dashed line for bulk Er[1], and the concentrations of Ho are listed.

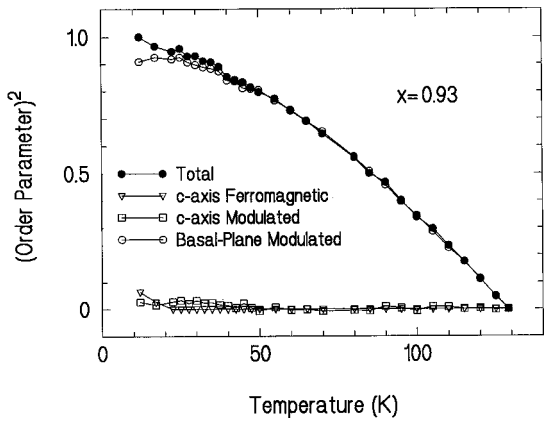

FIG. 3. The square of the ordered components of the magnetic moments for the alloy $Ho_{0.93}Er_{0.07}$.

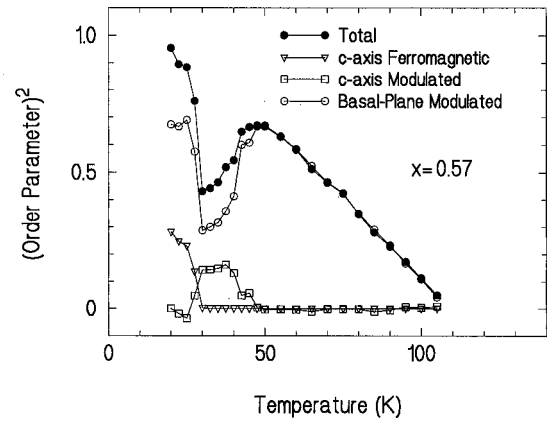

FIG. 5. The square of the ordered components of the magnetic moments for the alloy $Ho_{0.57}Er_{0.43}$.

wave-vector transfer $\boldsymbol{Q}$ of the neutrons.[18] The integrated intensity of the Bragg scattering at (0 0 2) was found to be independent of temperature showing that this scattering is nuclear scattering. The absence of any magnetic scattering in this region indicates that none of the samples have a ferromagnetic structure in which the magnetic moments are ordered in the basal plane perpendicular to $\boldsymbol{Q}$. In contrast, the intensity at the (1 0 0) Bragg position increases for all of the samples below about 25 K, showing that they have ordered magnetic moments along the c axis at low temperatures.

The intensity of the magnetic scattering measured with a wave-vector transfer $\boldsymbol{Q}=(0\ 0\ 2-q)$ is proportional to the ordered moment perpendicular to $\boldsymbol{Q}$,[18] namely, in the basal plane, so that

$$I(0\ \ 0\ \ 2-q)=F_1[\langle S_x(q)\rangle^2+\langle S_y(q)\rangle^2], \tag{1}$$

where F_1 is a constant depending on the form factor, fundamental constants and the instrumental parameters. The intensity of the Bragg scattering when $\boldsymbol{Q}=(1\ 0\ q)$ is given by

$$I(1\ \ 0\ \ q)=F_2[0.01\langle S_x(q)\rangle^2+\langle S_y(q)\rangle^2+0.99\langle S_z(q)\rangle^2], \tag{2}$$

where F_2 is a constant similar to F_1 and the numerical constants are deduced from the component of the ordered moments perpendicular to $\boldsymbol{Q}$. The temperature-dependent part of the scattering at the (1 0 0) Bragg reflection is given by

$$I_M(1\ \ 0\ \ 0)=F_3\langle S_z(0)\rangle^2, \tag{3}$$

where F_3 is another constant. Since the wave-vector transfers (1 0 0) and (1 0 q) are very similar, the changes in the magnetic form factors and instrumental conditions between these two wave-vector transfers are small and if they are neglected $F_3=2F_2$. A detailed calculation gives $F_3=2.05F_2$.

The experimental results were then analyzed by assuming that $\langle S_x(q)\rangle^2=\langle S_y(q)\rangle^2=\frac{1}{2}\langle S_\perp(q)\rangle^2$. This is the case for the magnetic structures such as the basal-plane helix or cone which are isotropic about the c axis, and for all other structures if it is assumed that there are randomly populated domains throughout the films. The ratio of F_1 to F_2 was determined experimentally from the intensities measured for $\boldsymbol{Q}=(0\ 0\ 2-q)$ and (1 0 q) for phases in which $\langle S_z(q)\rangle$ is known to be zero. Typically $F_1=0.28F_2$ which is also consistent with calculations. As is conventional, the square of the ordered components $\langle S_\perp(q)\rangle^2$, $\langle S_z(q)\rangle^2$, and $\langle S_z(0)\rangle^2$, were then normalized to the square of the total ordered moment $\langle S_T\rangle^2$ at low temperatures where $\langle S_T\rangle^2=\langle S_\perp(q)\rangle^2+\langle S_z(0)\rangle^2+\langle S_z(q)\rangle^2$ and the results for the five samples are shown in Figs. 3–7. The different magnetic structures that are to be identified from the measurements are as follows.

(a) Basal-plane helix: $\langle S_\perp(q)\rangle\neq 0$, $\langle S_z(q)\rangle=0$, $\langle S_z(0)\rangle=0$.

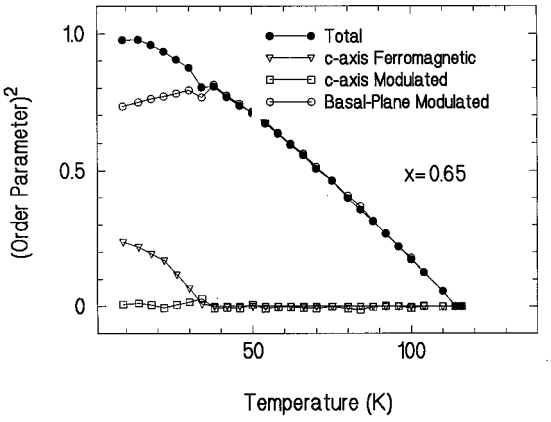

FIG. 4. The square of the ordered components of the magnetic moments for the alloy $Ho_{0.65}Er_{0.35}$.

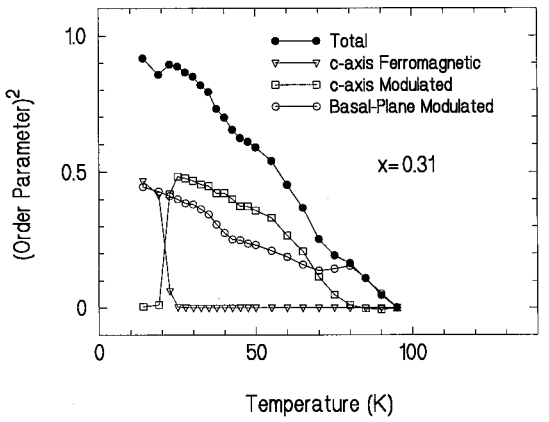

FIG. 6. The square of the ordered components of the magnetic moments for the alloy $Ho_{0.31}Er_{0.69}$.

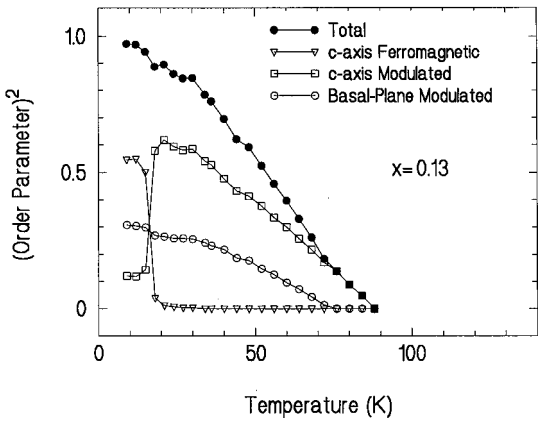

FIG. 7. The square of the ordered components of the magnetic moments for the alloy $Ho_{0.13}Er_{0.87}$.

(b) Tilted helix: $\langle S_\perp(q)\rangle \neq 0$, $\langle S_z(q)\rangle \neq 0$, $\langle S_z(0)\rangle = 0$, $R = |\langle S_z(q)\rangle|/|\langle S_\perp(q)\rangle| < 1$.

(c) Cycloid. $\langle S_\perp(q)\rangle \neq 0$, $\langle S_z(q)\rangle \neq 0$, $\langle S_z(0)\rangle = 0$, $R = |\langle S_z(q)\rangle|/|\langle S_\perp(q)\rangle| > 1$.

(d) Cone: $\langle S_\perp(q)\rangle \neq 0$, $\langle S_z(q)\rangle = 0$, $\langle S_z(0)\rangle \neq 0$, $\tan\theta = \langle S_z(0)\rangle/\langle S_\perp(q)\rangle$.

(e) c-axis longitudinally modulated: $\langle S_\perp(q)\rangle = 0$, $\langle S_z(q)\rangle \neq 0$, $\langle S_z(0)\rangle = 0$.

The identification of the tilted helix and the cycloid requires further discussion. These two phases are different because the titled helix has components of the ordered moments along the three perpendicular directions $\langle S_x\rangle$, $\langle S_y\rangle$, and $\langle S_z\rangle$. In contrast the cycloid has ordered moments in only one direction in the basal plane. Despite this difference, if there is a random set of cycloid domains the scattering from these two phases is indistinguishable because both have $\langle S_\perp(q)\rangle$ and $\langle S_z(q)\rangle$ nonzero. These phases do have different higher harmonics but the scattering from these was not observable in the experiments.

The identification of the tilted helix and the cycloid was therefore performed by using symmetry arguments and the results of the Landau theory described in Sec. IV. The experiments show that the temperature dependence of the intensities is continuous except for some of the transitions to the conical phase. Since the symmetry group of the tilted helix is a subgroup of the symmetry group of the basal-plane helix, whereas that of the cycloid is not a subgroup, the transition from a basal-plane helix to a tilted helix can be continuous while that from a basal-plane helix to a cycloid must be of first order. We can therefore identify the phase for which $\langle S_z(q)\rangle$ is small compared to $\langle S_\perp(q)\rangle$ as a tilted helix. The Landau theory predicts that the continuous transition between a tilted helix and a cycloid occurs when $R = |\langle S_z(q)\rangle|/|\langle S_x(q)\rangle| = 1$. We have used this result to identify the transition from the experimental data. A more refined theory might give a different critical value of R, but it is unlikely to alter the phase diagram qualitatively.

Similarly, symmetry considerations indicate that the c-axis longitudinally modulated phase can have a continuous transition to a cycloid but not to a tilted helix. The sequence of continuous transitions is then basal-plane helix $\leftrightarrow$ tilted helix$\leftrightarrow$cycloid$\leftrightarrow$$c$-axis longitudinally modulated.

III. MAGNETIC STRUCTURES

A. Experimental results

The experimental results were analyzed as described in the previous section. Except for a few limited temperature ranges, the widths of the peaks were independent of the temperature and determined by the experimental resolution showing that the magnetic order is of long range and has an extent of at least 2000 Å in the growth direction of the alloy. For each sample the integrated intensities of the observed peaks were used to determine the square of the total ordered moment, the square of the modulated component in the basal plane and along the c axis, and the square of the ferromagnetic component along the c axis, Figs. 3–7, in units such that the square of the total ordered moment is one at low temperatures. The statistical errors are smaller than the size of the points. Close to the Néel temperature for the onset of magnetic ordering the square of the ordered moments increases approximately linearly with the temperature difference from T_N. The Néel temperature was therefore obtained from a linear extrapolation of the measured intensities. The magnetic structures for each sample are described in the next sections and summarized in Table II. The transition temperatures from, for example, a helix to a cycloid are written as T_{HC}, where the first symbol refers to the high-temperature phase and the second to the stable phase at lower temperatures. The symbols P, H, T, C, D, L, and Co refer to the paramagnetic, helical, tilted helical, cycloidal, disordered, c-axis longitudinally modulated, and conical phases, respectively.

B. Results for $x = 0.93$

Magnetic ordering is observed below $T_{PH} = 128.9 \pm 0.4$ K and the absence of a c-axis longitudinally modulated component, Fig. 3, shows that the structure is a basal-plane helix. The wave vector on ordering q_0 is 0.279, which is very similar to that found for pure Ho. On cooling the sample, the wave vector decreases steadily as shown in Fig. 2 and the behavior resembles that of a pure Ho film. Below $T_{HCo} = 20 \pm 1$ K the wave vector has the commensurate value of 0.200 and the alloy has a conical structure. The cone opening angle is 90° at T_{HCo} and decreases smoothly on cooling to 75 $\pm 2°$ at 12 K. This suggests that the transition from the helical to the conical structure is continuous. In the temperature range between 45 and 20 K there is perhaps a trace of a nonzero $\langle S_z(q)\rangle$ component but this is, at most, 3.5% of the basal-plane component, and so it is probably not significant. If the structure was a tilted helix the tilt would be at most 2°.

Higher-order harmonics are observed at low temperatures for the conical structure corresponding to the fifth and seventh harmonics of the first order wave vector with intensities of 0.9 and 0.3 % of the main magnetic peak, respectively. The presence of these higher harmonics confirms the lock-in to a commensurate value with a (122) structure, where each 1 or 2 denotes the number of planes with their moments aligned approximately along successive easy axes in the basal plane.

The decrease in the Néel temperature from that of pure Ho and the existence of a helical structure are to be expected.

More surprising is the occurrence below T_{HCo} of a conical phase. The conical phase is suppressed for similar pure Ho films grown on Y (Ref. 9) and the modulation wave vector $q=0.20$ is different from that of the conical structure of pure bulk Ho for which $q=0.167$.

C. Results for $x=0.65$

The experimental results for the $x=0.65$ sample are shown in Figs. 2 and 4. The Néel temperature is $T_{PH}=113.5\pm0.5$ K, with an ordering wave vector of 0.281, and the ordered structure is a basal-plane helix. The wave vector decreases steadily on cooling and below $T_{HCo}=35\pm1$ K the structure becomes a cone with a cone angle that decreases smoothly with temperature. The wave vector at T_{HCo} is 0.233 and decreases on cooling until it locks in to 0.224 ± 0.002 below 24 ± 1 K. This wave vector is, within error, $\frac{2}{9}$ which corresponds to a (121212) commensurate structure. Both fifth and seventh harmonics are observed in the scattering at 9 K with intensities of 1.8 and 0.6 % of the primary scattering. These results are very similar to those of the $x=0.93$ sample, but with T_{PH} decreased and T_{HCo} increased. The only qualitative change is that the wave vector locks in to a commensurate value at a lower temperature than the onset of the conical structure at T_{HCo}, whereas for the $x=0.93$ sample the wave vector was temperature independent throughout the conical phase.

D. Results for $x=0.57$

For the $x=0.57$ sample the onset of magnetic order is at $T_{PH}=109\pm0.5$ K with the moments ordering in the basal plane (Fig. 5). The modulation wave vector is $q_0=0.282$ at T_{PH} and decreases steadily on cooling as shown in Fig. 2. Between T_{PH} and approximately 50 K the total moment increases smoothly, before reaching a plateau region between 50 and 40 K. We note that the plateau region appears to coincide with the wave vector passing through the commensurate value of $q=\frac{1}{4}$, and that in this temperature interval the basal-plane moments decrease and the c-axis moments order in a continuous fashion. We identify this as the phase transition from the basal-plane to tilted helix.

On cooling below 40 K the surprising result is found that the total integrated intensity appears to decrease down to 30 K. At the same time the square of the c-axis longitudinally modulated component is roughly one half of that of the square of the basal-plane moment. This indicates that the moments are ordered isotropically in all three crystallographic directions. Moreover, in this temperature regime, the widths [full width at half maximum (FWHM)] of the magnetic peak at $(0\ 0\ 2-q)$ is 0.0154 Å^{-1}, compared with 0.0126 Å^{-1} outside this interval. This shows that the magnetic order in this temperature region is not long range, but has a domain size of about 700 Å. We have therefore designated this phase as the disordered phase. This identification is supported by a comparison of our results with those obtained for bulk crystals as discussed in Sec. IV. This phase has not been found in bulk rare earths, is incommensurate with a wave vector less than 0.25, and is isotropic.

Below $T_{DCo}=30.0\pm1.0$ K, the structure changes to a long-range ordered cone and there is a rapid increase in the square of both the total moment and the basal-plane moment. The results, shown in Fig. 5, suggest that most of the moment is ordered in the conical phase. The angle of the cone decreases steadily on cooling and is $57.1\pm1.0°$ at 20 K, while the modulation wave vector of the conical phase is 0.230, and decreases with decreasing temperature. Higher-order satellites were not observed.

E. Results for $x=0.31$

Magnetic ordering for the $x=0.31$ sample is observed for temperatures below $T_{PH}=95\pm0.5$ K, as shown in Fig. 6. The wave vector at the onset of helical basal-plane ordering is $q_0=0.282$, Fig. 2. The c-axis components of the magnetic moments order below $T_{HT}=81\pm1$ K and increase steadily in magnitude, while the basal-plane components remain approximately constant. The structure is probably a tilted helix above $T_{TC}=65\pm3$ K, at which temperature the basal-plane component of the moment $\langle S_\perp(q)\rangle$ is 0.97 that of the c-axis $\langle S_z(q)\rangle$ moment. On further cooling, the total ordered moment steadily increases while the ratio of the c-axis to basal-plane moment R increases to 1.27 at 40 K and then decreases to 1.10 at 25 K. Since the c-axis moment is larger than the basal-plane moment, the structure of this phase for the reasons discussed in Secs. II C and IV A is probably a cycloid. The ratio R decreases towards one on cooling so as to maximize the total ordered moment on every atomic plane. The wave vector is constant, within error, at a value of $q=0.250$ below 35 K. Below $T_{CCo}=22\pm2$ K the magnetic structure changes to a conical structure with a an opening angle constant at $45\pm1°$, and a wave vector for the basal-plane component of 0.237 which is the same as that of the conical phase of bulk Er. The opening angle of the cone is almost independent of temperature, and a substantial fraction of both the cycloidal and conical phases are present between 24 and 20 K. We have therefore concluded that $T_{CCo}=22\pm2$ K. The results are consistent with a sharp jump in the wave vector between these two phases, and so this and the temperature independence of the cone angle suggest that the transition is of first order. Higher harmonics were not observed in the scattering from the conical phase for this sample.

F. Results for $x=0.13$

The sample with $x=0.13$ is magnetically ordered below $T_{PL}=88\pm0.5$ K and the wave vector at the onset of order is $q_0=0.284$. The structure is c-axis longitudinally modulated and similar to that observed for bulk Er at high temperatures. Below $T_{LC}=73.6\pm1.0$ K when the wave vector has increased to 0.285, the basal-plane components order and the modulation wave vector decreases. The ratio of the c-axis longitudinally modulated component to the basal-plane moment reduces with decreasing temperature and is constant at 1.24 below 48 K. This cycloid locks in with a wave vector of 0.25 below 27 ± 1 K. Below $T_{CCo}=16.5\pm1.0$ K, the scattering gives evidence of both a conical structure and a small c-axis longitudinally modulated component of the ordered moment, as shown in Fig. 7. A consistent explanation of the results is that the sample has regions of both cycloid and conical structures . If we assume that the fraction of the film

with the cycloidal structure is determined by the c-axis longitudinally modulated component, and that the ratio of c-axis to basal-plane moments for the cycloid is fixed at 1.24 as found between 48 and 20 K, then the data suggest that the cone opening angle is independent of temperature at $39.5 \pm 0.3°$. The proportion of the film with the cycloidal structure is 0.93 at 18 K, 0.15 at 15 K, and 0.10 below 12 K. Although there is no increase in the width of the $(0\ 0\ 2-q)$ magnetic peak below 20 K, there is an increase in the width of the $(1\ 0\ q)$ peak to 0.024 $Å^{-1}$ at 15 K from 0.016 $Å^{-1}$ at 25 K. This is consistent with the c-axis longitudinally modulated component of the scattering arising from a thin region of the sample of about 500 Å thick. Above 15 K the wave vectors of the $(0\ 0\ 2-q)$ and $(1\ 0\ q)$ peaks are the same. Below 15 K they differ and the wave vector of the $(1\ 0\ q)$ scattering is consistent with it arising solely from a cycloid with $q=\frac{1}{4}$. The wave vector of the $(0\ 0\ 2-q)$ peak is smaller indicating that the basal-plane ordering of the cone has a wave vector $q=0.241$. We conclude, therefore, that the sample has two distinct magnetic structures below 16 K, with about 90% of the sample exhibiting a conical structure similar to that of bulk Er but with a cone angle of 39.5° instead of 30°, and the remainder of the sample adopting a cycloidal structure with a ratio of the c-axis longitudinally modulated to basal-plane moment of 1.24. Since Er films grown on Y substrates do not have a conical phase,[8] it is likely that this sample is very close to the boundary for the onset of the conical phase. Possibly the cycloid occurs in a thin layer next to the Y seed where the film is most highly strained, while the cone occurs in the less highly strained part of the sample away from the seed.

IV. PHASE DIAGRAM

A. Landau theory

In this section, the extent to which the experimental results and particularly the phase diagram can be described by a Landau theory will be discussed. This approach is expected to be appropriate at temperatures close to the magnetic ordering temperature. The experimental results suggest that except at the lowest temperatures, the magnetic ordering of the ith plane is well described by a simple sinusoidal order parameter of the form

$$\langle S_{i\alpha}\rangle = S\sigma_\alpha \cos(q\cdot R_i+\phi_\alpha), \tag{4}$$

where σ_α is a variable which varies between 0 and 1 depending on the structure and the temperature and S is the averaged magnetic moment. The Landau expansion of the free energy averaged over each atomic site is then given by Jensen and Mackintosh[19] as

$$F-F_0=\sum_\alpha a(T-T_N)\sigma_\alpha^2+\sum_{\alpha\beta} u[2+\cos 2(\phi_\alpha-\phi_\beta)]\sigma_\alpha^2\sigma_\beta^2 + d\sigma_z^2+v\sigma_z^4, \tag{5}$$

where the first two terms are isotropic and arise largely from the exchange interactions. They are given approximately by[19]

$$a=\left(\frac{3}{4}\right)\frac{S^2}{S(S+1)}k_B, \tag{6}$$

and

$$u=\left(\frac{9}{160}\right)\frac{S(S^2+S+1/2)}{(S+1)^3}k_BT. \tag{7}$$

The parameter T_N is given by

$$T_N=\frac{1}{3}\left[S(S+1)K(q)+\frac{d}{a}\right], \tag{8}$$

where $K(q)$ is the Fourier transform of the exchange constant and q is the wave vector at which the transform is a maximum. The anisotropic terms d and v, which arise from the crystal field and from any anisotropy in the exchange interactions, are the lowest order terms in a power series expansion of these effects. The coefficient d is negative for Er and positive for Ho and so the average value of d is expected to pass through zero for Ho/Er alloys. This expression for the free energy describes the interactions between the basal planes and the parameters should be calculated by averaging over the different interactions: Ho-Ho, Ho-Er, and Er-Er. This approximation is appropriate because the intraplanar exchange constants are strong and for the heavy rare earths they align the magnetic moments parallel so that each plane can be treated as having a constant average magnetic moment. This approach differs from that developed earlier[15,16] in which the Ho and Er magnetic moments order independently with their own moment directions and interacting with an average environment which was obtained self-consistently. We have assumed that the strong intra-planar interactions result in the whole of each basal plane behaving as a unit.

The Landau expansion of the free energy, Eq. (5), is given by Jensen and Mackintosh.[19] However, it has not been discussed in detail as the parameter d passes through zero, and so we shall first describe this behavior. If $d>0$, while $v>0$, there is a transition at $T_{PH}=T_N$ from a paramagnetic phase to a helix with $\sigma_x=\sigma_y=\sigma_H$ and $\phi_x=\phi_y\pm\pi/2$. The phase relationship results from the minimization of the second term of Eq. (5) when $u>0$. The order parameter in the helix is given by

$$\sigma_H^2=\left(\frac{a}{8u}\right)(T_N-T) \tag{9}$$

and

$$F-F_0=-\left(\frac{a^2}{8u}\right)(T_N-T)^2. \tag{10}$$

If $d<0$ and $v>-u/3$, a transition occurs at a higher temperature

$$T_{PL}=T_N-\frac{d}{a}, \tag{11}$$

with $\sigma_x=\sigma_y=0$ while $\sigma=\sigma_z$ and the phase is c-axis longitudinally modulated with

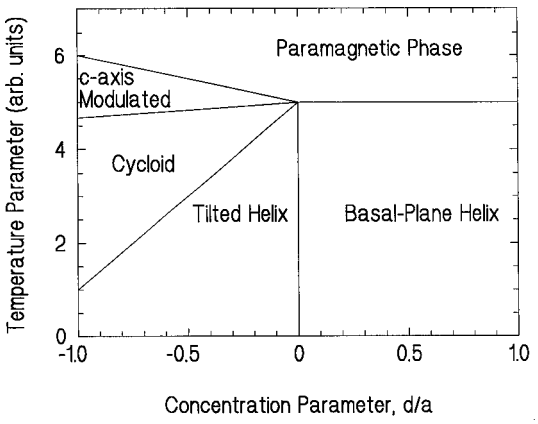

FIG. 8. Schematic phase diagram deduced from Landau theory by assuming that only d/a varies with concentration and that the other parameters in the theory are temperature and concentration independent. The structure of the different magnetic phases is indicated in the figure.

$$\sigma^2=\left(\frac{a}{6u+2v}\right)(T_{PL}-T). \tag{12}$$

The free energy is given by

$$F-F_0=-\left(\frac{a^2}{12u+4v}\right)(T_{PL}-T)^2. \tag{13}$$

On cooling, this phase becomes unstable against the formation of a cycloid in which $\sigma_x=\sigma_1$, $\sigma_z=\sigma_3$, and $\phi_x=\phi_z \pm \pi/2$, where since this approximation to the free energy is isotropic in the basal plane, the choice of a component in the x direction is arbitrary. The transition between the c-axis longitudinally modulated phase and the cycloid is continuous and occurs at a temperature of

$$T_{LC}=T_N+\frac{du}{a(2u+v)}. \tag{14}$$

Detailed expressions can be obtained for the temperature dependence of σ_1 and σ_3.

The transition between the cycloid and the helix occurs through an intermediate structure with three components $\sigma_x = \sigma_1$, $\sigma_y=\sigma_2$, and $\sigma_z=\sigma_3$ with $\phi_x=\phi_z$ or $\phi_z+\pi$. Special cases of this phase are the cycloid with $\sigma_2=0$, the basal-plane helix with $\sigma_3=0$, and the tilted helix. The stability of the helix against σ_3 shows that if $v>0$, the transition between the helix and tilted helix is continuous and occurs when $d=0$ at T_{HT}, while if $v<0$ the transition is of first order and occurs for $d<2$. The boundary between the tilted helix and the cycloid occurs when the cycloid is unstable against σ_2, which occurs for $v>0$ when

$$T_{TC}=T_N+4\left(\frac{ud}{va}\right), \tag{15}$$

and σ_1 and σ_3 of the cycloidal phase are equal or $R=1$ as described in Sec. II C.

Detailed expressions can be obtained for the temperature dependence of the free energy and of the σ's for all of the phases.

The phase diagram is illustrated schematically in Fig. 8 for $v>0$ as a function of temperature and d/a. We have assumed that $K(q)$ is a constant and that $u/v=1$. The phase diagram is unusual in that it shows a pentacritical point at $T=T_N$ and $d=0$ with five different phases coexisting: paramagnetic, helical, tilted helical, cycloidal, and a c-axis longitudinally modulated. This is distinct from the tetracritical points which occur in nearly isotropic three-dimensional systems with commensurate order parameters and for systems with competing anisotropies for which the structures are simple ferromagnets or antiferromagnets. If $v<0$, the tilted helix is unstable and there is a first-order transition between the cycloid and the helix; while if $v<-3u$, higher-order terms are needed to stabilize the c-axis longitudinally modulated structures and the properties depend on the details of these higher-order terms.

We have not considered the effect of critical fluctuations on this pentacritical point for two reasons. First, the critical phenomena of bulk Ho is not yet understood[20] and secondly, the mean-field-like behavior of the order parameter in our results suggests that critical fluctuations may play only a small role in describing the global properties of the phase diagram of Ho/Er alloys. In order to apply these results to Ho/Er alloys, the simplest possible average crystal assumption is that the parameters vary linearly with the concentration from Ho to Er.

B. Concentrations

Most of the physical properties of Ho and Er are very similar. As discussed in Sec. II A, the lattice parameters differ by less than 0.5%, the atomic numbers and hence x-ray form factors by 1.5% and the nuclear coherent-scattering lengths for neutron scattering by 0.6%. The magnetic properties do, however, change considerably with the concentration as discussed above, and so it is preferable to use these properties as a measure of the concentration.

One of the most direct measures of the concentration is the magnetic ordering temperature, and the results of Sec. III together with the Landau theory were used to deduce the concentrations of the different samples. The theory and the magnetization measurements of Bozorth *et al.*[12] suggest that T_{PH} is linearly dependent on the concentration between pure Ho and the pentacritical point as predicted by the Landau theory. Their results[12] suggest that the transition temperature (in K) is given by

$$T_{PH}=77+56x. \tag{16}$$

The measurements of the transition temperature then enable the concentrations for four of the samples to be obtained and the results are listed in Table II, where they are compared with the nominal values. The phase boundary between the helix and tilted helix is predicted by Landau theory to be linear in the concentration and the experimental results suggest that $T_{HT}=-138.5x+125.33$. The intersection between these two boundaries gives the pentacritical point at $T=91 \pm 2$ K and $x=0.25\pm0.02$. The phase boundaries for the onset of the c-axis longitudinally modulated phase T_{PL} and of the transition to the cycloid T_{LC} are assumed from Landau theory to be linear in the concentration between this critical point and the phase transitions of pure Er, and hence

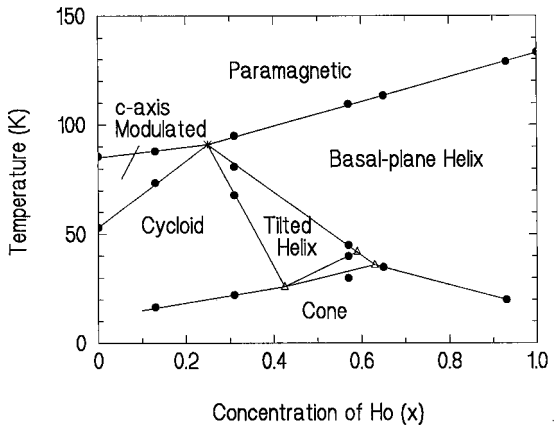

FIG. 9. The magnetic phase diagram for Ho/Er alloys. The solid lines show the phase boundaries between different magnetic structures, and the cross at $T=91$ K and $x=0.25$ shows the position of the pentacritical point. The region enclosed by the lines between the open triangles is the region over which the disordered phase may occur as described in the text.

$$T_{LC}=53+152x, \tag{17}$$

$$T_{PL}=85+24x. \tag{18}$$

The corresponding transition temperatures of the most Er-rich sample can then be used to deduce its concentration as 0.13 ± 0.02 and the agreement obtained from the two boundaries provides some support for the methodology.

Two of the samples, $x=0.57$ and $x=0.93$, have concentrations which are substantially different from the nominal concentrations, Table II. A comparison can, however, be made with measurements[12–15] for bulk crystals. T_{PH} was measured to be 125 K for a bulk crystal with a nominal concentration of 0.9,[15] and a value of 121 K was obtained for a powder sample of nominal concentration 0.8.[12] It is therefore reasonable that the sample with $T_{PH}=128.5$ K has a concentration of 0.93. Similarly, $T_{PH}=104$ and 106 K have been obtained for bulk crystals with x nominally 0.5,[12,16] and so our sample with $T_{PH}=109.6$ K probably has $x=0.57$, somewhat higher than the nominal concentration of 0.5. The samples with concentrations of 0.57 and 0.93 were grown using the same calibration, and the results are consistent with this calibration being slightly in error, resulting in an Er concentration which was low.

C. Phase diagram at high temperatures

The results discussed in Sec. III and listed in Table II are combined with the Landau theory described in Sec. IV A to obtain the phase diagram for the Ho/Er alloys as shown in Fig. 9. The points show the phase transition temperatures, deduced from the measurements, and the lines between the different phases are given by the equations for T_{PH}, T_{HT}, T_{LC}, and T_{PL}. The phase boundary between the cycloid and the tilted helix is determined approximately by the pentacritical point and the one experimental point as

$$T_{TC}=-330x+173.5. \tag{19}$$

There are five different magnetic phases which meet at the pentacritical point and for all of the four ordered phases the wave vector varies continuously.

Although the phase diagram deduced from the experiments and shown in Fig. 9 is topologically the same as the one obtained schematically from Landau theory, Fig. 8, there are notable differences. First, the transition temperature for the onset of magnetic order steadily decreases with decreasing x. This is because the exchange interaction $K(q)$ varies with x as well as the anisotropy parameter. The concentration dependence of T_{PH} [Eq. (16)] and T_{PL} [Eq. (18)] can be described by the model if in units of temperature

$$\frac{d}{a}=-8+32x, \tag{20}$$

while Eq. (8) suggests that the exchange constant, in units of temperature, varies as

$$K(q)=2.57+1.06x. \tag{21}$$

The exchange constants depend[19] on the de Gennes factors $(g-1)^2J(J+1)$ multiplied by the conduction electron susceptibility $\chi(q)$ and the interaction between the conduction electrons and the $4f$ electrons I. Equation (21) suggests that the peak of $I^2\chi(q)$ is 1.26 ± 0.05 times larger for Er than for Ho, and occurs at a wave vector of 0.284 instead of 0.280.

Mean field analysis of the continuous transition between the helix and tilted helix shows that it occurs when $d=0$. The phase diagram shown in Fig. 8 was calculated by assuming that d is independent of temperature and depends solely on the concentration. The experimental points for the phase boundary T_{HT}, Fig. 9, depend on concentration showing that the anisotropy constant d varies both with concentration and temperature. This is to be expected because the crystal field generates contributions to d from the terms B_2^0, B_4^0, and B_6^0, which do not have the same temperature dependencies.[19] Furthermore, the temperature dependence of the lattice parameters tends to make the ratio of the lattice parameters (c/a) larger as the temperature decreases, thereby reducing the anisotropy constant.

If the temperature variation of d is assumed to be linear with $T_{PH}-T$ in the helical phase, then the equation for the phase boundary between the helix and the tilted helix suggests that Eq. (20) should be modified to include the temperature dependence of d as

$$\frac{d}{a}=-8+32x-0.165(T_{PH}-T). \tag{22}$$

A comparison with the equation for the phase boundary between the tilted helix and the cycloid, Eq. (19), then suggests that

$$u/v=3.05\pm0.3. \tag{23}$$

When this Landau theory is extended to calculate the boundary between the c-axis longitudinally modulated phase and the cycloidal phase T_{LC} the value of T_{LC} for $x=0$ is 73 K which is much larger than the value for pure Er of 53 K. This failure of the model may result from the temperature

TABLE III. Temperature dependence of the order parameter near the Néel temperature.

x	0.13	0.31	0.57	0.65	0.93
$\sigma^2/(T_N-T)$	0.0113 (20)	0.0125 (10)	0.0125 (10)	0.0129 (10)	0.0116 (10)

dependencies of the parameters of the free energy of the c-axis longitudinally modulated phase being different from those of the helical phase.

The Landau theory can also be compared with the values of the order parameter close to the Néel temperature. In Table III, the values of $\sigma^2/(T_{PH}-T)$ are listed and are approximately constant throughout the helical phase at 0.0124 ± 0.0008, which for the model suggests that $u/a = 10.1 \pm 0.7$ K. In the c-axis longitudinally modulated phase, $\sigma^2/(T_{PL}-T)$ is smaller than for the helix which is inconsistent with Eqs. (10) and (13) and $v<u$. It is, however, consistent with the behavior of T_{LC} described above, because the transition to the cycloid occurs when the order parameter of the c-axis longitudinally modulated phase reaches a critical value. If the order parameter increases more slowly than that calculated by the model, the phase transition will occur at a lower temperature. Figure 10 shows a calculation of the temperature dependence of the different components of the magnetization for the $x = 0.31$ sample using the model described above. The parameters were $a=0.68$ from Eq. (6), $u=6.87$ K deduced from the average increase of the order parameter in the helix, d/a as given by Eq. (22), and $v=2.25$ K from Eq. (23). The results are qualitatively similar to the experimental results in Fig. 6.

The values of the parameters for the Landau theory can be compared with other estimates. At the pentacritical point the expansion of the Brillouin function gives $u=4.07$ K. At T_{PH}, the anisotropy parameter d arises from the crystal-field term B_2^0, and from the anisotropic dipolar interactions. B_2^0 has recently been estimated as 0.024 meV (Ref. 21) for Ho and -0.027 meV^2 for Er, while the anisotropy of the dipolar interactions is 0.035 meV (Ref. 19) for both Ho and Er. These results give $d/a = 34$ K for Ho and -15 K for Er. These latter values are somewhat different from our estimates of 24 and -8 K, respectively, and they suggest that the multicritical point occurs when $x=0.31$ which is in reasonable agreement with our experiments.

In conclusion, Landau theory gives a semiquantitative description of the behavior of Ho/Er alloys close to the onset of magnetic ordering. The parameters are within factors of 2 of the values expected from theory and other measurements. The model successfully describes the helix and tilted helix but is less satisfactory for the c-axis longitudinally modulated phase.

D. Phase diagram at low temperatures

At low temperatures all of the alloys have a conical phase in which the wave vector varies with concentration and is often locked in to a commensurate value at low temperatures. Figure 11 shows the wave vector and cone angle at sufficiently low temperature and both vary smoothly with concentration and can be extrapolated to $x=0$ and $x=1$ to give the properties of the conical phases in the bulk. The phase boundaries are probably continuous between the helical and the conical phases, and of first order between the tilted helix or cycloid and the cone.

The concentration dependence of the maximum total ordered moment and the calculated atomic moment gJ is shown in Fig. 12. The former were obtained by comparing the integrated intensity of the $(0\ 0\ 2-q)$ scattering with that of the (0 0 2) nuclear Bragg peak and correcting for the form factor and the Lorentz factor. The very reasonable agreement between the theory and experiment, given the uncertainties of this type of measurement arising from interference from the seed and capping layers, suggests that the magnetic moments are mostly ordered at low temperatures.

At low temperature the theory differs from that in Sec. IV A because the term in the free energy due to the entropy [the u term in Eq. (5)] is small and the free energy becomes

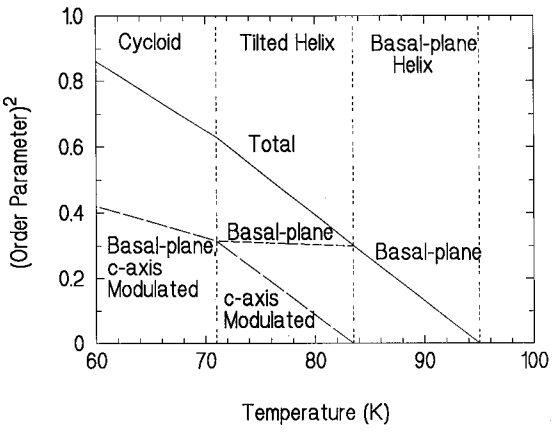

FIG. 10. The temperature dependence of the square of the order parameters for $Ho_{0.31}Er_{0.69}$ as calculated by the Landau theory for the basal-plane helical, tilted helical, and cycloidal phases. In the cycloidal phase both basal-plane and c-axis components are equal.

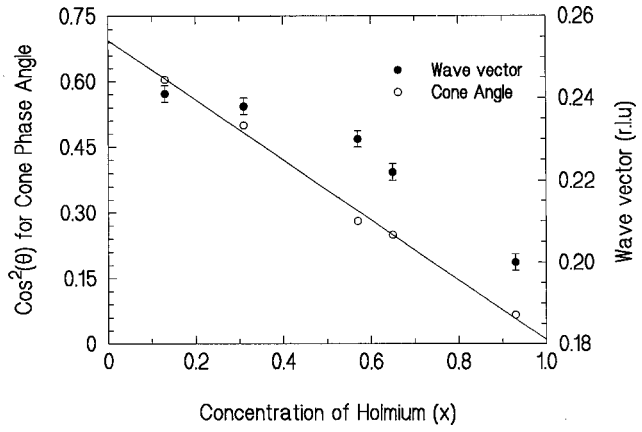

FIG. 11. The modulation wave vector at low temperatures for the basal-plane components in the conical phase (c^*) and the square of the cosine of the cone angle. The solid line is a straight line fit to the latter to deduce the parameters of the Landau theory.

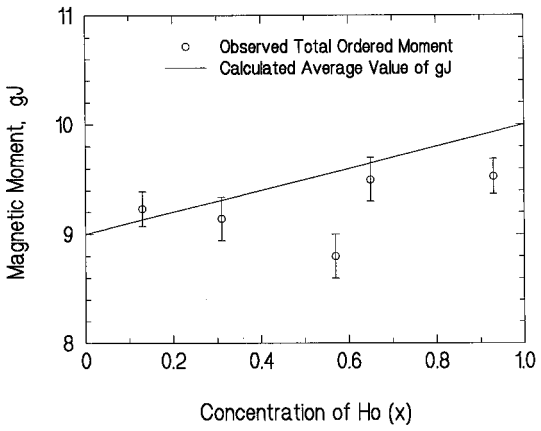

FIG. 12. The total ordered magnetic moment as determined experimentally (points) and the average moment gJ (solid line) of the alloys. Note that the zero of the scale is suppressed.

the same as the energy of the system. For a system with a sinusoidal variation of the ordered moment with position, the energy is given by

$$E=-\frac{1}{2}\sum_{\alpha} K(q)\sigma_{\alpha}^{2}(q)+\frac{1}{2}d\sigma_{z}^{2}(q)+\frac{3}{8}v\sigma_{z}^{4}(q), \quad (24)$$

where we have neglected the anisotropic terms of sixth and higher order in the ordered moment. If the ordered moment is uniform in space the energy is

$$E=-\sum_{\alpha} K(0)\sigma_{\alpha}^{2}(0)+d\sigma_{z}^{2}(0)+v\sigma_{z}^{4}(0). \quad (25)$$

The order parameters at low temperature are determined for the classical theory with the condition that the total moment $\sigma_T=1$, and the quantum fluctuations are neglected. The incommensurate phases have the properties

(a) Helix:

$$\sigma_x(q)=\sigma_y(q)=1, \quad E_H=-K(q).$$

(b) Tilted Helix:

$$\sigma_x(q)=1, \quad \sigma_y(q)=\cos\theta, \quad \sigma_z(q)=\sin\theta,$$

$$E_T=-K(q)-\frac{d^2}{6v}, \text{ while } \sin^2\theta=\frac{-2d}{3v}.$$

(c) Cycloid:

$$\sigma_x(q)=\sigma_z(q)=1, \quad E_C=-K(q)+\frac{d}{2}+\frac{3v}{8}.$$

The stable phase is a helix if $d>0$, a tilted helix if $-3v/2<d<0$, and a cycloid if $d<-3v/2$.

The experimental results described in Sec. III show that the most stable phase for all of the alloys at low temperature is a conical phase for which the model gives

$$\sigma_x(q)=\sigma_y(q)=\sin\theta, \quad \sigma_z(0)=\cos\theta,$$

and

$$E_{Co}=-K(q)-\frac{(\delta+d)^2}{4v},$$

where $\delta=K(q)-K(0)$ and $\cos^2\theta=-(\delta+d)/2v$. The phase boundary between the cone and the helix is continuous and occurs when

$$\delta=-d, \quad (26)$$

while that between the tilted helix and cone is of first order and occurs when

$$\delta=\left(\sqrt{\frac{2}{3}}-1\right)d. \quad (27)$$

The jump in the cone angle at the tilted helix-to-cone transition is given by

$$\cos^2\theta_0=\frac{-d}{\sqrt{6}v}. \quad (28)$$

The phase boundary between the cone and cycloid is of first order and occurs when

$$\delta=-d-v\left(-\frac{2d}{v}-\frac{3}{2}\right)^{1/2}, \quad (29)$$

while the jump in the cone angle is

$$\cos^2\theta_0=\frac{1}{2}\left(-\frac{2d}{v}-\frac{3}{2}\right)^{1/2}. \quad (30)$$

These results can be used to construct a schematic phase diagram by varying the parameters δ, d, and v. The parameter δ describes the difference between the exchange constant $K(q)$ for a modulated structure and that for a ferromagnetic structure $K(0)$. As the temperature is lowered the wave vector decreases, Fig. 2, and the difference between $K(0)$ and $K(q)$ becomes smaller. Furthermore there are magnetoelastic and dipolar contributions[19] to $K(0)$ which further decrease the difference so that in bulk Ho, for example, $K(0)$ is larger than $K(q)$ even though the exchange part of the interaction is still a minimum for an incommensurate value of q. Since q increases with the concentration of Er, Fig. 2, δ can be expected to increase with increasing x. The cone angle varies smoothly with the concentration, Fig. 11, suggesting that both δ and d vary linearly with x. The multicritical point at which the cone, helix and tilted helix meet occurs when $\delta=d=0$. If it is assumed that d/v varies with both temperature and concentration while δ/v varies only with the concentration, the experimental results for the cone angle and the multicritical point suggest that

$$\frac{d}{v}=1.88(x-0.9)+t \quad (31)$$

and

$$\frac{\delta}{v}=-0.48(x-0.63), \quad (32)$$

where t is a scaled temperature. The schematic phase diagram resulting from these assumptions is shown in Fig. 13 and it has a region of stability for all of the phases observed

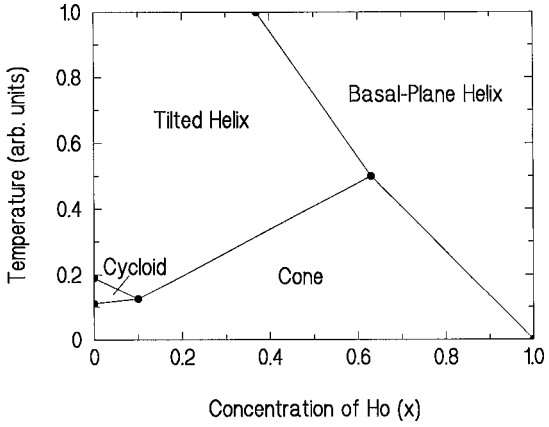

FIG. 13. The phase diagram at low temperatures deduced from an approximate expression for the energy of the alloys.

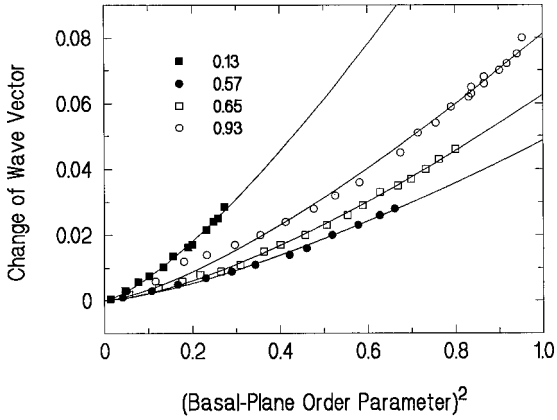

FIG. 14. The change of the ordering wave vector from that at the onset of ordering, as a function of the square of the ordered basal-plane moment for four of the alloys. The fifth alloy with $x=0.31$ gives a more complicated temperature dependence. The solid lines are fits to a power law and describe the results satisfactorily.

in the experiments. The calculated phase boundary of the tilted helix has a much larger region of stability than is observed while the cycloid has a smaller region. Better agreement between the theory and the experimental results in Fig. 9 can be obtained by including the higher order crystal-field terms, and allowing all of the parameters to vary with both temperature and concentration. We shall not describe the results here as the theories involve more parameters which are difficult to calculate.

A commensurate phase is observed with $q=\frac{1}{4}$ over an appreciable part of the phase diagram, Fig. 9, in both the cycloidal and tilted helical phases and at temperatures just above the transition to the conical phase. In contrast, if this wave vector occurs in either the helical or conical phases, this commensurate phase is stable over only a very narrow temperature interval if at all. This lock-in arises because of the crystal-field anisotropy through the $v\sigma_z^4(q)$ term and the additional terms of this form which can arise if $4q$ is a reciprocal lattice vector. Since this term only contributes to the energy if there is a c-axis longitudinally modulated contribution to the order parameter, it does not produce any effect on the conical or helical phases. At low temperatures the conical phase has a commensurate modulation of the basal-plane moments with the commensurate wave vector varying with the concentration. These commensurate phases arise from the crystal-field anisotropy within the basal planes and the structures are similar to those observed in other studies of the heavy rare earths.

E. Temperature dependence of the ordering wave vector

The mean field theories described in the previous sections do not account for the change in the modulation wave vector with temperature. At the onset of ordering the wave vector is nearly the same, Fig. 2, for all the alloys as for bulk Ho and Er, showing that the conduction electron susceptibilities have maxima at very similar wave vectors. At lower temperatures the wave vectors differ, and the theory for these changes was developed by Elliott and Wedgwood[23] who showed that the magnetic ordering splits the conduction electron energy bands at the Fermi level, and that for a helix the energy is a minimum if the wave vector decreases as the ordered moment increases. For bulk Ho, Ho/Y, and Ho/Lu alloys, the change in the wave vector below T_N, Δq, is approximately proportional to the cube of the ordered moment[24] but this behavior is not understood in detail.

The Ho/Er alloys have a variety of different magnetic phases and so it is of interest to study the change in the wave vector for the different phases. First, as found in bulk Er (Ref. 1), the wave vector increases slightly on cooling below the ordering temperature in the c-axis longitudinally modulated phase. Since the band splitting arises in both the spin-up and spin-down conduction bands, no large change is to be expected in the wave vector of the maximum of the susceptibility. Second, there is a marked temperature dependence of Δq with temperature for the helical phases as shown in Fig. 14. The results for the samples with $x=0.57$, 0.65, and 0.93 are described at least approximately by

$$\Delta q = 0.091x \times \sigma^n, \tag{33}$$

where $n=2.8\pm0.2$. This behavior is similar to that found for the helical phases of Ho, Ho/Y, and Ho/Lu alloys and it is surprising only in that it is proportional to x, the concentration of the Ho atoms.

Third, Fig. 14 also shows that the change in the wave vector in the cycloidal phase of the $x=0.13$ sample is a simple function of the ordered moment in the basal plane. A fit to the results gives $\Delta q=0.15\sigma_x^n$ with the exponent $n=2.6\pm0.2$. This exponent is similar to that observed in the helical phase but the amplitude is very different. The theory of the band splitting for the cycloid is similar to that for the helix if the band structure is isotropic in spin space. The observed difference in the amplitudes suggests that the interactions are not isotropic and that it is necessary to take account of the spin-orbit effects on the band structure. Finally, the behavior of q for the sample with $x=0.31$ is complex, and we have been unable to find a simple connection with either the basal-plane moment or the total moment. Given that the sample has four different magnetic structures this failure is unsurprising. Likewise the simple power law for the helix fails for the $x=0.57$ sample when it enters the tilted

helical and disordered phases. We conclude that further work is needed to understand the temperature dependence of the wave vector.

F. Comparison with other experiments

Bozorth *et al.*[12] made magnetization measurements on five different Ho/Er bulk alloys and the magnetization when a magnetic field was applied along the different crystallographic axes. The results can be compared with our measurements of the temperature for the onset of magnetic order T_{PH} and the temperature of the transition to a conical phase T_{HCo} as a function of the concentration. In Sec. IV B, we have used these measurements to obtain our concentrations and so the results are consistent with the concentrations listed in Table II. The measurements[12] of T_{HCo} and T_{CCo} gave slightly higher temperatures than those listed in Table II especially when the concentrations were small or close to 1. For example, Bozorth *et al.* obtained 26 K when $x=0.2$, whereas for $x=0.31$ we obtain 22 K. This difference probably arises because basal-planes of the thin films are clamped as described for thin films of Ho and Er in Sec. I.

A single crystal with a nominal concentration of 0.9 was also studied by Rønnow.[15] The scattering was consistent with the magnetic structure being a basal-plane helix between 125 and 24 K and a conical structure at lower temperatures. At 10 K the cone angle was 76.4° and the modulation wave vector $\frac{7}{36}$. One advantage of performing experiments on bulk samples is that weak higher harmonics can be observed when the intensity is only 10^{-4} of the strongest reflections, whereas with the thin films the higher harmonics must be 2×10^{-3} of the strong reflections to be readily observable. Consequently the higher harmonics in the $x=0.9$ bulk sample were studied in detail and careful fits to the data showed that the $q=\frac{7}{36}$ conical structure had a disordered arrangement of the spin slips. The wave vector of this phase 0.1944 is smaller than for the conical phase of the thin film with $x=0.93$, Table II.

Powder samples with $x=0.7$ and 0.4 were studied by Shirane and Pickart.[13] They suggested that the magnetic structure was a basal-plane helix just below the onset of long-range order and then transformed to a cone at low temperatures. The modulation wave vector and the cone angle were in good agreement with those found for the conical phase of our thin films. A phase diagram of Ho/Er alloys was first proposed by Millhouse and Koehler.[25] It differs from that shown in Fig. 8 because the nature of the cycloid phase was not then understood or distinguished from the tilted helical phase, while the isotropic disordered phase was not observed, and the multicritical point between these phases and the paramagnetic phase occurred at somewhat smaller concentration. We consider that these differences arise largely because of the better data and samples now available. The phase diagrams reported for Tb/Er alloys[26] and Dy/Er alloys[25] are similar in that the nature of the cycloid was not then known and so the identification of a mixed phase and of a tilted helical phase needs to be treated with caution. We suspect that the Er-rich parts of these phase diagrams are very similar to those found for Ho/Er, shown in Fig. 9.

A crystal with $x=0.5$ has been studied with neutron-scattering techniques by Shirane and Pickart,[13] Howard and Bohr,[14] and by Rønnow[15] and with magnetic resonant x-ray-scattering techniques by Pengra *et al.*[16] Shirane and Pickart observed the transitions to the helical phase at T_{PH} and to the conical phase for which they obtained values for the modulation wave vector and cone angle that are in agreement with those reported above. The later experiments also observed intermediate phases in agreement with the results shown in Fig. 5 and described in Sec. III D. Qualitatively the results for the high- and low-temperature ordered phases are the same as those described above for the film with $x=0.57$. The neutron scattering in the intermediate disordered phase between 47 and 33 K is, however, different. On cooling the intensity of the $(0\ 0\ 2-q)$ peak increased, while for the thin film it decreases, and simultaneously for the bulk the intensity of the $(1\ 0\ q)$ peak increased. These results suggest that there was a considerable increase in the total ordered moment in this phase with substantially less ordered moment in both the helical and conical phases.

We consider that this direct conclusion is not physically reasonable but that the results can be understood if the bulk crystal has a disordered phase similar to that proposed for the $x=0.57$ film in Sec. III D. In this case the disordered phase causes a relief of the extinction in the bulk crystal so that although the ordered moment does not increase the scattering does increase. It is well known[2,6] that extinction strongly reduces the neutron-magnetic scattering in bulk single crystals of Ho and Er and this is another illustration of the difficulty of obtaining reliable intensities of strong magnetic reflections from bulk rare-earth crystals. Although the structure initially proposed[14,16] for the intermediate phase of bulk $x=0.5$ samples are different from our disordered phase, more recently Rønnow[15] has also proposed that extinction might play an important role. If our model of this intermediate phase as a disordered phase is correct, it deserves more attention. It is completely surrounded in the phase diagram by phases which have long-range order, and occurs in both bulk crystals and films.

We have been unable, so far, to measure the phase boundaries between this phase and the neighboring helix, tilted helix, and cone; and so the phase diagram is still uncertain in this area. The phase is not described by a mean field theory of the structures. The short-range order has an incommensurate wave vector. The short-range ordered moments are nearly isotropic. It is therefore an example of a $d=3$, $n=6$ system with random anisotropy. At the critical point between the helix, cone, and tilted helix the average values of both the anisotropy d and exchange parameter δ are zero, and so there are local and random fluctuations about zero in the values of both of these parameters due to the statistical fluctuations in the concentration. It is therefore a random anisotropy system with the further complication of fluctuations to the conical phase. In systems with competing anisotropies and simple antiferromagnetic ordering $n=d=3$ the fluctuations[22] do not destroy the long-range order. Randomness does, however, have a much larger effect on systems with continuous symmetry such as incommensurate systems. These have low-energy phase fluctuations which can couple to the random fluctuations leading to a destruction of long-range order. Clearly further theoretical work is needed to understand this aspect of the phase diagram.

V. SUMMARY AND CONCLUSIONS

We have measured the magnetic structures of thin single crystal films of Ho/Er alloys. The samples were grown by MBE techniques and are of high crystallographic quality. Neutron-scattering measurements were made to determine the different magnetic structures and seven different structures were identified. Besides the paramagnetic structure, we have observed a helical structure similar to that found in bulk Ho, a c-axis longitudinally modulated structure, and a cycloid similar to those found for bulk Er, and at low temperatures we identified a conical structure similar to those found in bulk Ho and Er even though the same conical structure is suppressed in similar thin films of the pure materials.

In addition, we have observed two phases which do not occur in the pure materials. Between the helical and cycloidal phases there is a tilted helical phase in which all three components of the magnetization are ordered and nonzero. It is also suggested that there is a disordered phase with only short-range magnetic order completely surrounded in the phase diagram, Fig. 9, by phases which, within our resolution, have long-range order. Similar phases have not been observed in other commensurate systems with competing anisotropies.

The results have been used to construct a phase diagram which is shown in Fig. 9. The phase diagram is complex so that even when neglecting the transitions between similar commensurate and incommensurate phases there are three different multicritical points. A pentacritical point occurs at the intersection of five phases, the properties of which have not been explored before, and two bicritical points, one of which is at the intersection of two continuous phase transition lines and a first-order line, and another of which is at the intersection of two first-order lines with a continuous phase transition line. In Sec. IV C we have shown that a Landau description of the behavior close to the onset of long-range order describes the properties semiquantitatively at least above 40 K. In Sec. IV D we have used an approximation to the energy to discuss the low-temperature properties and have shown that such a theory has the necessary ingredients to account for the observed phases. Progress is dependent on the development of further theory. First, it is necessary to develop the statistical mechanics of the pentacritical point and of the isotropic disordered phase with $n=6, d=3$, and random anisotropy. Second, there is the need to calculate the concentration and temperature dependence of the parameters in the Landau theory so that it provides an accurate representation of the phase diagram. Third, although the average model used in this paper appears to be adequate for describing most of the properties of the alloys, further work is needed to justify this type of model. Fourth, there is not an adequate understanding of the temperature dependence of the modulation wave vector in the alloys or for the pure materials.

ACKNOWLEDGMENTS

We have benefited from helpful discussions with J. Jensen, H. M. Rønnow, and the late A. R. Mackintosh, and from excellent technical support while performing the experiments. Financial support at Oxford was provided by the EPSRC and at Risø by the Large Scale Facilities Program of the EU.

[1] J.W. Cable, E.O. Wollan, W.C. Koehler, and M.K. Wilkinson, Phys. Rev. A **140**, 1896 (1965).
[2] R.A. Cowley and J. Jensen, J. Phys.: Condens. Matter **4**, 9673 (1992).
[3] W.C. Koehler, J.W. Cable, M.K. Wilkinson, and E.O. Wollan, Phys. Rev. **151**, 414 (1966).
[4] D. Gibbs, D. Harshman, E. Isaacs, D. McWhan, D. Mills, and C. Vettier, Phys. Rev. Lett. **61**, 1241 (1988).
[5] D. Gibbs, J. Bohr, J.D. Axe, D.E. Moncton, and K.L. D'Amico, Phys. Rev. B **34**, 8182 (1986).
[6] R.A. Cowley and S. Bates, J. Phys. C **21**, 4113 (1988).
[7] J.A. Simpson, D.F. McMorrow, R.A. Cowley, and D.A. Jehan, Phys. Rev. B **51**, 16 073 (1995).
[8] J.A. Borchers, M.B. Salamon, R.W. Erwin, J.J. Rhyne, R.R. Du, and C.P. Flynn, Phys. Rev. B **43**, 3123 (1991).
[9] D.A. Jehan, D.F. McMorrow, R.A. Cowley, R.C.C. Ward, M.R. Wells, N. Hagmann, and K.N. Clausen, Phys. Rev. B **48**, 5594 (1993).
[10] J.A. Simpson, R.A. Cowley, D.A. Jehan, R.C.C. Ward, M.R. Wells, D.F. McMorrow, K.N. Clausen, T.R. Thurston, and D. Gibbs, Z. Phys. B **101**, 35 (1996).
[11] J.A. Simpson, D.F. McMorrow, R.A. Cowley, D.A. Jehan, R.C.C. Ward, M.R. Wells, and K.N. Clausen, Phys. Rev. Lett. **73**, 1162 (1994).
[12] R. Bozorth, A. Clark, and J. van Vleck, Int. J. Magn. **2**, 19 (1972).
[13] G. Shirane and S.J. Pickart, J. Appl. Phys. **37**, 1032 (1966).
[14] B.K. Howard and J. Bohr, Phys. Scr. **T39**, 96 (1991).
[15] H.M. Rønnow, Masters thesis, University of Copenhagen, 1996.
[16] D. Pengra, N. Thoft, M. Wulff, R. Feidenhans'l, and J. Bohr, J. Phys.: Condens. Matter **6**, 2409 (1994).
[17] R.A. Cowley, R.C.C. Ward, M.R. Wells, M. Matsuda, and B. Sternlieb, J. Phys.: Condens. Matter **6**, 2985 (1994).
[18] S.W. Lovesey, *Theory of Neutron Scattering from Condensed Matter* (Oxford University Press, Oxford, 1984), Vol. 2.
[19] J. Jensen and A.R. Mackintosh, *Rare Earth Magnetism: Structures and Excitations* (Oxford University Press, Oxford, 1991).
[20] For a review, see, G. Helgesen, J.P. Hill, T.R. Thurston, and D. Gibbs, Phys. Rev. B **52**, 9446 (1995).
[21] J. Jensen, Phys. Rev. B **54**, 4021 (1996).
[22] S. Fishman and A. Aharony, Phys. Rev. B **18**, 3507 (1978).
[23] R.J. Elliott and F.A. Wedgwood, Proc. Phys. Soc. London **81**, 846 (1963).
[24] R.A. Cowley and J. Jensen, Mat. Fys. Medd. K. Dan. Vidensk. Selsk. **45**, 35 (1997).
[25] A.H. Millhouse and W.C. Koehler, Int. J. Magn. **2**, 389 (1971).
[26] H. Fujii, Y. Hashimoto, T. Okamoto, N. Achiwa, and S. Kawano, J. Phys. Soc. Jpn. **50**, 2939 (1981).